Fusion of SPECT and multidetector CT images for accurate localization of pelvic sentinel lymph nodes in prostate cancer patients

Fusion of SPECT and Multidetector CT Images for Accurate Localization of Pelvic Sentinel Lymph Nodes in Prostate Cancer Patients

Hiroto Kizu, PhD[1]; Teruhiko Takayama, MD[1]; Mamoru Fukuda, MD[2]; Masayuki Egawa, MD[2]; Hiroyuki Tsushima, PhD[1]; Masato Yamada, PhD[3]; Kenji Ichiyanagi, MD[4]; Kunihiko Yokoyama, MD[4]; Masahisa Onoguchi, MD[1]; and Norihisa Tonami, MD[4]

[1]Department of Radiological Technology, School of Health Science, Kanazawa University, Kodatsuno, Kanazawa, Japan; [2]Department of Integrative Cancer Therapy and Urology, Graduate School of Medical Science, Kanazawa University, Takaramachi, Kanazawa, Japan; [3]Department of Radiology, Kanazawa University Hospital, Takaramachi, Kanazawa, Japan; and [4]Department of Biotracer Medicine, Graduate School of Medical Science, Kanazawa University, Takaramachi, Kanazawa, Japan

Objective: The present study was performed to investigate the feasibility of fusion of images obtained by SPECT and multidetector CT (MDCT) for the accurate localization of sentinel lymph nodes in prostate cancer patients.

Methods: To facilitate the fusion of both SPECT and CT images, a pelvic MDCT scan was performed with 3 markers of small plastic bullets attached to the skin over the bilateral iliac crests and the ventral midline at the same height. SPECT was performed after the same locations were marked with needle caps containing ^{99m}Tc-pertechnetate. The images were superimposed by use of free software (MRIcro). The results of hot lymph node detection with fusion images were compared with those of surgery.

Results: The images could be successfully superimposed for all 11 patients examined. Surgeons accurately confirmed 27 (87.1%) of 31 regional lymph nodes on fusion images.

Conclusion: Fusion of SPECT and MDCT images is useful for the precise localization of sentinel lymph nodes in prostate cancer patients.

Key Words: fusion image; sentinel lymph node; prostate cancer; lymphoscintigraphy; CT

J Nucl Med Technol 2005; 33:78–82

The concept of the sentinel lymph node (SLN) is rapidly becoming accepted for assessing regional lymph node metastases for multiple tumors, including malignant melanoma (*1,2*), breast cancer (*3,4*), thyroid cancer (*5*), and gastrointestinal cancer (*6,7*). A sentinel node is defined as the lymph node first receiving lymphatic drainage from a tumor. It is most likely the site of early metastasis. The histopathologic findings for an excised SLN indicate the need for further dissection of the nodal basin if metastatic spread or micrometastases are found. Alternatively, if the SLN is tumor free, the nodal basin can be regarded as free of disease, and unnecessary dissection can be avoided. The results of SLN biopsy play an important role in the selection of both the appropriate surgical procedure and nonsurgical adjuvant therapy (*8*).

Although the rate of detection of an SLN is increased by the use of SPECT, it is difficult to precisely identify an SLN deeply located in an anatomic structure by means of SPECT alone. With the rapid development of endoscopic urologic surgery, lymphoscintigraphy and intraoperative γ-probes have become more important for the detection of the precise localization of SLNs. On the other hand, other imaging modalities, including CT and MRI, are excellent tools for the depiction of morphologic structures. At present, CT is the method of choice for the initial noninvasive evaluation of patients with suspected malignancy. Therefore, the fusion of SPECT and CT images is expected to allow the precise localization of SLNs. A hybrid SPECT/CT system can be used for SLN mapping in patients with malignant tumors (*8*). Because the use of such equipment is limited, we devised a method for generating fusion SPECT and CT images without requiring such equipment and for identifying the precise anatomic site of an SLN by comparison with the results of surgery.

The purpose of this study was to investigate the feasibility of fusion of SPECT and CT images for accurate SLN localization in prostate cancer patients.

For correspondence or reprints contact: Hiroto Kizu, PhD, Department of Radiological Technology, School of Health Science, Kanazawa University, 5-11-80 Kodatsuno, Kanazawa 920-0942, Japan.
E-mail: kizu@cf6.so-net.ne.jp

MATERIALS AND METHODS

Patient Population

Eleven patients with prostate cancer, diagnosed by biopsy, were enrolled in this study. Patients ranged in age from 60 to 75 y (mean ± SD, 67.5 ± 5.2 y). The average preoperative prostate-specific antigen level was 23.4 ± 20.8 ng/mL. Preoperative bone scans, CT scans, and MR images for all patients showed no evidence of bone metastasis or abdominal lymph node enlargement. Before examination, approval for the study protocol was obtained from the institution's ethical committee, and written informed consent was obtained from all patients.

Radiologic Examination

For the detection of metastasis, a pelvic multidetector CT scan was obtained with a Light Speed Ultra 16 scanner (GE Healthcare). Before imaging, 3 small plastic bullets (~5 mm in diameter) were attached as landmarks on the skin over the bilateral iliac crests and the ventral midline at the same height (Fig. 1A). A CT scan was performed under the following conditions: tube voltage, 120 keV; the product of tube current and time, 200 mA; field of view, 35 cm; slice thickness, 5 mm, with no slice gap; detector configuration, 16 × 1.25; beam collimation, 20 mm; pitch, 0.562:1; and speed, 11.25 mm per rotation. A complete acquisition lasted approximately 13 s.

Radionuclide Study

A radionuclide study was performed with 74 MBq of ^{99m}Tc-phytate (Daiich Radioisotope Laboratories Ltd.) dissolved in a volume of 0.1–0.2 mL. The radiotracer was injected transrectally into each lobe of the prostate under ultrasound guidance (Color Doppler SDD2200; Aloka Co. Ltd.) with a 15-cm-long 21-gauge needle (PEIT needle; Hakko Medical Co. Ltd.). Immediately before imaging, the patient's skin was marked in the same places with needle caps containing 0.2 MBq of ^{99m}Tc-pertechnetate (Fig. 1B). At 15 min after injection, an anterior planar image was recorded in the supine position on a single-head γ-camera (Orbiter; Siemens Medical Solutions). The counts on the planar image were collected for 10 min in a 256 × 256 matrix with a high-resolution, low-energy parallel collimator. The energy was centered at 140 keV with a 20% window for ^{99m}Tc. SPECT images were obtained after the second planar imaging 3 h after injection with a triple-head γ-camera (GCA-9300A/HG; Toshiba Medical Systems). Data acquisition was performed in a 128 × 128 matrix for 50 s each for a total of 60 frames in steps of 6° over 360° with a GMS 5500A/PI imaging system (Toshiba Medical Systems). The total acquisition time was 20 min.

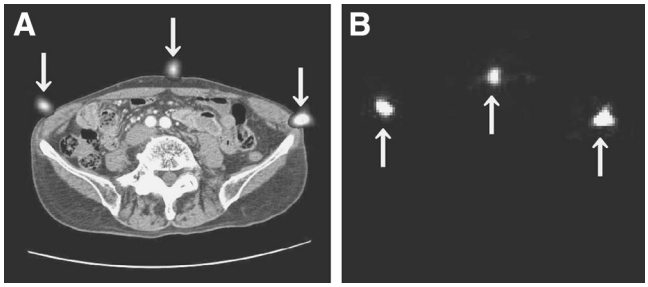

FIGURE 1. Landmarks (arrows) on axial slices of CT (A) and SPECT (B).

For data analysis, the pixel truncation method was used to exclude the effects of high levels of activity at the injection site (*9*). The cutoff value was 300 counts in most cases, although it was changed as necessary in some cases. The data were reconstructed by use of an iterative method based on an ordered-subset expectation maximization algorithm (3 iterations and 10 subsets) (*10*). No prefilter was used. The images were interpreted by 2 nuclear medicine physicians. Counts on images were not measured.

Image Fusion Technique

Free viewing software, MRIcro (*11*), was installed on a personal computer (PC) (FMV DESKPOWER C5/86WL; Fujitsu Ltd.) running the Windows Me operating system (Microsoft Corp.). MRIcro can create Analyze format headers for exporting images to other platforms. The CT data were entered into the PC as Digital Imaging and Communications in Medicine data by use of a read-only memory compact disk, and the SPECT data were entered into the PC online by use of free software (FFFTP version 1.92; Sota Jun). The CT and SPECT data, converted to Analyze format, were superimposed on the display. We set matrix dimension, pixel size, and slice thickness for SPECT and multidetector CT images in MRIcro to adjust the images of the 2 modalities. By moving cursor lines through the landmarks on both images, we adjusted the locations of both images so that the patient's body contours overlapped as correctly as possible. To obtain optimal alignment, hot spots caused by the skin markers on the SPECT images were manually overlapped with the plastic bullets on the CT images, and the prostate in the CT images and the injection site in the SPECT images were overlapped. To interpret the accurate localization of regional hot lymph nodes, fusion images were reconstructed in 3 views: axial, coronal, and sagittal slices.

Surgical Procedure

Approximately 5–6 h after the radionuclide study, the patients underwent endoscopic minilaparotomy because this surgical procedure is becoming standard for such patients at our institution (Fig. 2). The procedure requires only a single longitudinal excision (~5 cm long) several centimeters above the pubic bone and is therefore minimally invasive compared with conventional open surgery. A hand-held γ-probe (Navigator GPS; Tyco Healthcare Japan) was used to search for deeply located hot lymph nodes, which were then excised. After the excision, the radioactivity in the excised specimens was counted with the γ-probe, and the specimens were subjected to histopathologic examination. Ex vivo probing radioactivity of each lymph node counted for 10 s. The level of radioactivity in the aorta was used as

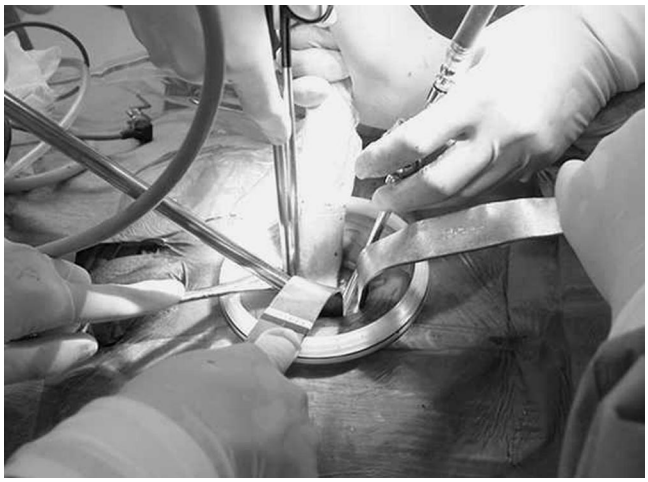

FIGURE 2. Endoscopic lymphadenectomy by means of minilaparotomy.

the background count level. A hot lymph node was defined as a node-to-background count density ratio determined to be higher than 2 by in vivo probing and a radioactivity of greater than 10 counts per 10 s (1 cps) of ex vivo probing (*12*).

RESULTS

SPECT and CT images were successfully fused for all patients, and fusion processing took approximately 20 min to complete. Table 1 shows the numbers, sizes, and counts of regional hot lymph nodes. Thirty-one hot lymph nodes were detected in the 11 patients. In 2 patients (cases 7 and 8), hot lymph nodes could not be visualized clearly on scintigraphy; however, these lymph nodes were detected by intraoperative γ-probing. Most of the lymph nodes were smaller than 1 cm, although the dimensions were not measured in 2 patients. Radioactivity in the excised specimens ranged from 1 to 3,556 cps. Histopathologic examination revealed nodal metastasis in case 2 (Table 1).

Correlation of the lymph node sites on fusion images and during surgery showed excellent agreement: 13 (100%) of 13 external iliac lymph nodes, 8 (100%) of 8 internal iliac lymph nodes, and 6 (85.7%) of 7 obturator lymph nodes. However, in 1 patient (case 1), there was a discrepancy between the site of the hot obturator lymph node on the fusion image and the actual site detected during surgery. This hot lymph node was detected successfully with the γ-probe. In this case, the discrepancy in the results occurred because the lymph node had been moved inward by manipulation during surgery.

Figures 3 and 4 show the hot left external iliac and right obturator lymph nodes, respectively. SPECT and CT images were fused successfully. Because the fusion images accurately revealed the existence of regional hot lymph nodes before surgery, these lymph nodes could be identified efficiently with the γ-probe. Because histopathologic examination detected metastasis in the external lymph node in case 2, the patient received radical surgery with enlarged lymphadenectomy and hormone therapy.

DISCUSSION

A precise diagnosis of lymph node metastasis status is essential for staging of disease, selection of the appropriate treatment procedure, monitoring of the response to treatment, and early detection of recurrence (*5,13*). Moreover, the lymph node metastasis status is a major prognostic factor, and patients with cancer confined to the primary site show better survival than those with lymph node metastases. Although extended lymph node dissection is the most precise and reliable stage evaluation method, this approach

TABLE 1
Surgically Excised Regional Hot Lymph Nodes in 11 Patients

	Size, mm × mm (cps), of the following lymph node*:					
	External iliac		Internal iliac		Obturator	
Case	R	L	R	L	R	L
1	(252)		(1,740)			(110)
2		6 × 4 (717)†			10 × 7 (10)	
3						6 × 4 (34), 3 × 2 (4)
4						8 × 5 (522)
5	5 × 5 (196)			6 × 4 (12)		
6	(1,673)	(105)			(220)	
7						5 × 3 (3)‡
8			9 × 6 (1)‡		4 × 3 (2)‡	
9	9 × 4 (62)	2 × 2 (27)	5 × 4 (698)	4 × 3 (372)		
10	5 × 5 (10), 7 × 5 (41)	8 × 7 (179), 10 × 8 (695)		4 × 4 (853)	7 × 5 (684)	
11	15 × 10 (430)	8 × 7 (3,556)	3 × 3 (349), 4 × 3 (56)	2 × 2 (11)		
Total	7	6	5	4	4	5

*Size measurements were not obtained for all lymph nodes. Totals represent numbers of lymph nodes.

†Positive for lymph node metastasis.

‡Not detectable by lymphoscintigraphy.

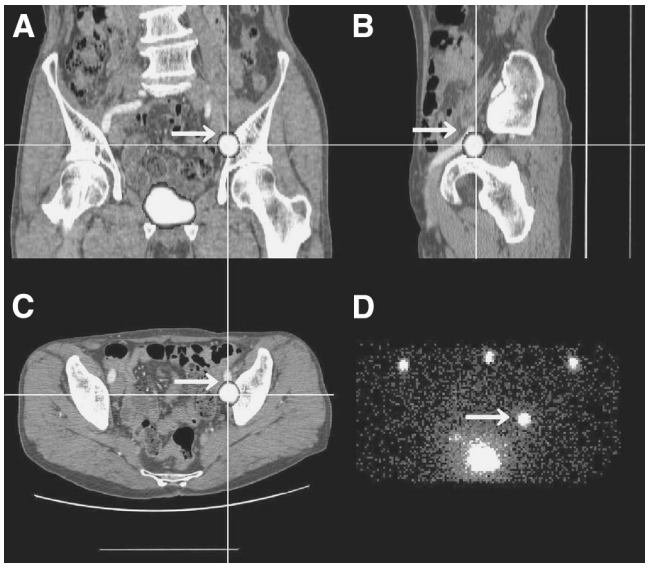

FIGURE 3. Fusion of SPECT and CT images indicating left external iliac lymph node (arrow) in case 2. (A) Coronal slice. (B) Sagittal slice. (C) Axial slice. (D) Anterior planar lymphoscintigraphic image.

is invasive. CT, MRI, and PET are used in the initial noninvasive evaluation of patients with suspected malignancy. However, CT and MRI do not allow definite determination of the presence of lymph node micrometastases (*10*). Furthermore, even PET with ^{18}F-FDG appears to be insufficiently sensitive to identify nodal micrometastases (*14*). The histopathologic findings for SLNs can represent the metastasis status of all regional lymph nodes with high accuracy. Many authors have reported the feasibility of SLN biopsies for malignant tumors, including malignant melanoma (*1,2*), breast cancer (*3,4*), thyroid cancer (*5*), squamous cell carcinoma of the head and neck region (*8*), and gastrointestinal tumors (*6,7*). However, there have been few reports regarding the identification of a hot lymph node in prostate cancer. Wawroschek et al. (*15,16*) concluded that hot lymph node identification is feasible not only in breast cancer and malignant melanoma but also in prostate cancer with a comparable technique.

In the present study, we tried to identify the SLNs in prostate cancer patients. Because intrapelvic lymph nodes may be located deeply along the blood vessels and because lymphatic drainage in this region is highly complex, it is difficult to determine the number of draining basins accurately. In addition, although the use of SPECT increases the rate of detection of hot lymph nodes, it is difficult to determine the anatomic localization of deep pelvic lymph nodes without also using other modalities. Hot lymph nodes situated superficially, as in breast cancer or skin malignant melanoma, are easily detected intraoperatively with a γ-probe, but it is difficult to detect deeply situated hot lymph nodes.

Recently, Tadokoro et al. (*17*) introduced a new urologic surgical method called minilaparotomy or portless endoscopic urologic surgery. This method requires only a single longitudinal incision above the pubis, is less invasive than conventional laparoscopic radical prostatectomy, and moreover is much less invasive than open surgery (*18*). With the application of this surgical technique, preoperative detection of hot lymph nodes is becoming more feasible, because it permits the surgeon to search efficiently with the γ-probe as long as fusion images provide precise anatomic localization. A hybrid SPECT/CT system can be used for SLN mapping in patients with malignant tumors (*8*). However, such specialized, expensive equipment is in limited use. Therefore, we investigated the feasibility of producing fusion images without the use of such equipment.

In the present study, CT was performed to search for lymph node metastases, and the data were reused with the intention of producing fusion images. This strategy is meaningful because it reduces the radiation doses to which patients must be exposed, compared to those used with a SPECT/CT system. Kretschmer et al. (*1*) investigated the fusion of SPECT and pelvic CT images for patients with malignant melanoma and concluded that it is an excellent tool for the precise localization of pelvic tumor-draining lymph nodes. Cense et al. (*7*) also reported that the combined use of CT and lymphoscintigraphy improves the precise localization of hot lymph nodes.

The scattering of γ-rays makes it more difficult to identify hot lymph nodes when they lie close to the injection site. Therefore, we applied pixel truncation and the ordered-subset expectation maximization reconstruction algorithm. These techniques were useful for reducing the artifacts in scintigraphy. In the present study, the anatomic sites of hot lymph nodes detected during surgery showed excellent agreement with those detected on the fusion images. In some patients, the surgeon found 2 or more affected lymph nodes, whereas scintigraphy showed only 1 hot lymph node. In some patients, scintigraphy did not identify the hot lymph

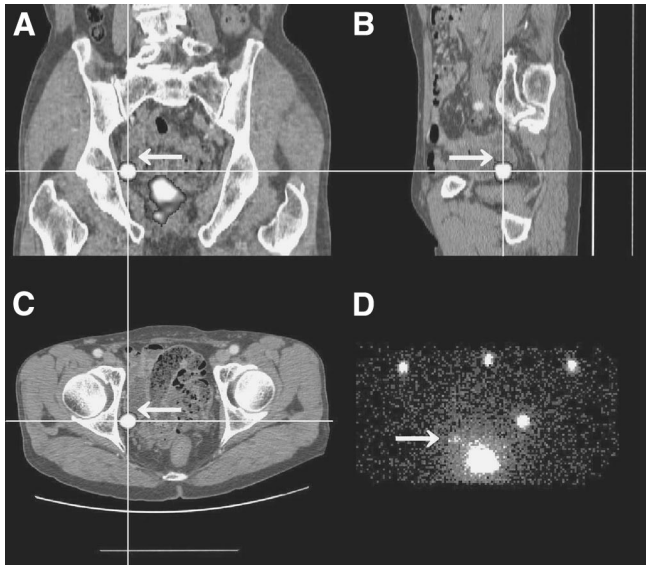

FIGURE 4. Fusion of SPECT and CT images indicating right obturator lymph node (arrow) in case 2. (A) Coronal slice. (B) Sagittal slice. (C) Axial slice. (D) Anterior planar lymphoscintigraphic image.

node, whereas the γ-probe allowed its identification. When the nodal count was less than 10 cps, it was difficult to detect hot lymph nodes by scintigraphy; however, the γ-probe could detect these nodes. The γ-probe revealed the presence of at least 1 hot lymph node in each patient. In case 1, there was a discrepancy between the site of the obturator hot lymph node on the fusion image and the actual site determined during surgery because the lymph node was moved inward by manipulation during surgery. To avoid such discrepancies between the fusion image and the actual site of the regional lymph node, care should be taken to reduce the movement of intraabdominal organs, respiratory movement during CT and SPECT, and movement of the lymph node from the original site by manipulation during surgery.

The results of hot lymph node detection in the present study were satisfactory because the fusion images predicted the site accurately for 27 (87.1%) of 31 regional lymph nodes.

CONCLUSION

The feasibility of fusion of SPECT and CT images was demonstrated, and this method was shown to be very useful for the precise localization of SLNs in patients with prostate cancer.

REFERENCES

1. Kretschmer L, Altenvoerde G, Meller J, et al. Dynamic lymphoscintigraphy and image fusion of SPECT and pelvic CT-scans allow mapping of aberrant pelvic sentinel lymph nodes in malignant melanoma. *Eur J Cancer*. 2003; 39:175–183.
2. Williams B, Hinkle GH, Douthit RA, Fry JP, Pozderac RV, Olsen JO. Lymphoscintigraphy and intraoperative lymphatic mapping of sentinel lymph nodes in melanoma patients. *J Nucl Med Technol*. 1999;27:309–317.
3. Yeung HWD, Cody HS III, Turlakow A, et al. Lymphoscintigraphy and sentinel node localization in breast cancer patients: a comparison between 1-day and 2-day protocols. *J Nucl Med*. 2001;42:420–423.
4. Alazraki NP, Styblo T, Grant SF, et al. Sentinel node staging of early breast cancer using lymphoscintigraphy and the intraoperative gamma detecting probe. *Semin Nucl Med*. 2000;30:56–64.
5. Israel O, Keider Z, Iosilevsky G, Bettman L, Sachs J, Frenkel A. The fusion of anatomic and physiologic imaging in the management of patients with cancer. *Semin Nucl Med*. 2001;31:191–205.
6. Fujii H, Kitagawa Y, Kitajima M, Kubo A. Sentinel nodes of malignancies originating in the alimentary tract. *Ann Nucl Med*. 2004;18:1–12.
7. Cense HA, Sloof GW, Klaase JM, et al. Lymphatic drainage routes of the gastric cardia visualized by lymphoscintigraphy. *J Nucl Med*. 2004;45:247–252.
8. Even-Sapir E, Lerman H, Lievshitz G, et al. Lymphoscintigraphy for sentinel node mapping using a hybrid SPECT/CT system. *J Nucl Med*. 2003;44:1413–1420.
9. Funahashi M, Shimonagata T, Mihara K, et al. Application of pixel truncation to reduce intensity artifacts in myocardial SPECT imaging with Tc-99m tetrofosmin. *J Nucl Cardiol*. 2002;9:622–631.
10. Leong LK, Kruger RL, O'Connor MK. A comparison of the uniformity requirements for SPECT image reconstruction using FBP and OSEM techniques. *J Nucl Med Technol*. 2001;29:79–83.
11. Rorden C, Brett M. Stereotaxic display of brain lesions. *Behav Neurol*. 2001;12:191–200.
12. Takasima H, Egawa M, Imao T, et al. Validity of sentinel lymph node concept for patients with prostate cancer. *J Urol*. 2004;171:2268–2271.
13. Czerniecki BJ, Bedrosian I, Faries M, Alavi A. Revolutionary impact of lymphoscintigraphy and intraoperative sentinel node mapping in the clinical practice of oncology. *Semin Nucl Med*. 2001;31:158–164.
14. Belhocine T, Pierard G, De Labrassinne M, Lahaye T, Rigo P. Staging of regional nodes in AJCC stage I and II melanoma: ^{18}FDG PET imaging versus sentinel node detection. *Oncologist*. 2002;7:271–278.
15. Wawroschek F, Vogt H, Wengenmair H, et al. Prostate lymphoscintigraphy and radio-guided surgery for sentinel lymph node identification in prostate cancer: technique and results of the first 350 cases. *Urol Int*. 2003;70:303–310.
16. Wawroschek F, Hamm M, Weckermann D, Vogt H, Harzmann R. Lymph node staging in clinically localized prostate cancer. *Urol Int*. 2003;71:129–135.
17. Tadokoro M, Masuda H, Okuno T, et al. Clinical study of surgical site infection following portless endoscopic urological surgery. *Acta Urol Jpn*. 2003;49:721–725.
18. Arai Y, Egawa S, Terachi T, et al. Morbidity of laparoscopic radical prostatectomy: summary of early multi-institutional experience in Japan. *Int J Urol*. 2003;10:430–434.